The Astrophysical Journal, 644: L000–L000, 2006 June 10

GAMMA-RAY IMAGING OF THE 2003 OCTOBER/NOVEMBER SOLAR FLARES

G. J. Hurford,[1] S. Krucker,[1] R. P. Lin,[1,2] R. A. Schwartz,[3] G. H. Share,[4,5] and D. M. Smith[6]

Received 2006 March 22; accepted 2006 April 24; published 2006 May 22

ABSTRACT

We present *RHESSI* imaging of three flares (2003 October 28 and 29 and November 2) in the 2.223 MeV neutron-capture gamma-ray line with angular resolution as high as 35″. Comparisons of imaged and spatially integrated fluences show that in all cases most, if not all, of the emission was confined to compact sources with size scales of tens of arcseconds or smaller that are located within the flare active region. Thus, the gamma-ray–producing ions appear to be accelerated by the flare process and not by a widespread shock driven by a fast coronal mass ejection. The 28 October event yielded the first such image to show double-footpoint gamma-ray line sources. These footpoint sources straddled the flaring loop arcade but were displaced from the corresponding 0.2–0.3 MeV electron-bremsstrahlung emission footpoints by 14″ and 17″ ± 5″. As with the previously studied 2002 July 23 event, this implies spatial differences in acceleration and/or propagation between the flare-accelerated ions and electrons.

Subject headings: gamma rays: observations — Sun: flares — Sun: X-rays, gamma rays

1. INTRODUCTION

Observations of gamma-ray line emission show that ions are accelerated up to ~MeV–GeV energies in large solar flares, whereas the solar energetic particles (SEPs) directly observed near 1 AU with comparable energies appear to be accelerated much higher (~2–40 $R_\odot$) in the solar atmosphere (Kahler 1994) by widespread shock waves driven by fast (>~1000 km s^{-1}) coronal mass ejections (CMEs). Almost all fast CMEs are associated with large solar flares, but the relationship between these two apparently separate ion accelerations is currently not understood. The energy contained in the flare-accelerated >~1 MeV ions can be comparable to that in flare-accelerated electrons (Ramaty et al. 1995; Ramaty & Mandzhavidze 2000). Both can carry a significant fraction (~10%–50%) of the total energy released in the flare (Lin & Hudson 1976; Lin et al. 2003; Emslie et al. 2004b, 2005). Until recently, gamma-ray line studies have been limited to spatially integrated spectroscopy (e.g., Share & Murphy 2004). Since 2002, however, NASA's *Reuven Ramaty High Energy Solar Spectroscopic Imager* (*RHESSI*; Lin et al. 2002) has provided the first capability for solar gamma-ray imaging as well as high-resolution spectroscopy of ion-produced gamma-ray lines and X-ray imaging spectroscopy of the bremsstrahlung radiation from energetic electrons.

The neutron-capture line at 2.223 MeV is the strongest of the many individual narrow and broad gamma-ray lines generated by accelerated ions (e.g., Ramaty et al. 1979; Smith et al. 2003). Accelerated ~10 to >~100 MeV $nucleon^{-1}$ protons and alpha particles colliding with the solar atmosphere produce fast neutrons that then thermalize in the photosphere before capture by ambient hydrogen to form deuterium, with the emission of an extremely narrow line (<~10 eV FWHM). Since the neutrons travel only a short distance (<~1″) during the ~100 s thermalization time (Hua & Lingenfelter 1987), images in the 2.223 MeV line indicate the site(s) of the original nuclear interactions.

The first gamma-ray line imaging (Hurford et al. 2003) showed that for the 2002 July 23 flare, the centroid of the 2.223 MeV line source was displaced by ~20″ from the corresponding centroid of the electron-bremsstrahlung continuum emission, a surprising result given the general similarity of the time profiles of electron-associated X-ray and ion-associated gamma-ray line emissions. Here we present 2.223 MeV line imaging for three intense flares that occurred during the solar activity of 2003 October/November.

2. OBSERVATIONS

RHESSI imaging (Hurford et al. 2002) uses nine bigrid rotating modulation collimators (RMCs) that provide logarithmically spaced angular resolutions between 2.″26 and 183″ FWHM. RMC 6 (35″) and RMC 9 (183″) have tungsten grids that are sufficiently thick (2 and 3 cm, respectively) to modulate photons at gamma-ray energies.

Behind each RMC is a cryogenically cooled (~80 K), electrically segmented germanium detector (Smith et al. 2002) that provides high spectral resolution (~1–10 keV FWHM) over the 3 keV–17 MeV energy range. The intense flux of 3 keV–0.2 MeV X-rays from strong flares stops primarily in the ~1 cm–thick front segments, allowing the higher energy gamma rays to be detected with minimal dead time by the ~7 cm–thick rear segments used in this work. As *RHESSI* rotates at ~15 revolutions per minute, the RMC transmissions vary rapidly. Imaging information is encoded in the resulting time modulation of the observed count rates. Telemetry includes the arrival time and energy of each detected photon, which, together with aspect information, enables the images to be reconstructed (Hurford et al. 2002). At 2.223 MeV, *RHESSI*'s spectral resolution (~6 keV FWHM) allows a narrow energy window (2.218–2.228 MeV) to be used to minimize background from the underlying continuum and to reject photons that Compton-scatter in the grids and elsewhere.

Following procedures outlined in Hurford et al. (2003), we reconstructed flare-averaged images using back projection for the 2.223 MeV neutron-capture line and 0.2–0.3 MeV electron-bremsstrahlung bands. Except where noted, both bands were imaged with RMCs 6 and 9 using the same aspect solution, imaging algorithms, and parameters (Table 1). This largely

[1] Space Sciences Laboratory, University of California, 7 Gauss Way, Berkeley, CA 94720-7450; ghurford@ssl.berkeley.edu, krucker@ssl.berkeley.edu, rlin@ssl.berkeley.edu.

[2] Department of Physics, University of California, Berkeley, CA 94720.

[3] NASA Goddard Space Flight Center/SSAI, Greenbelt, MD 20771; richard.schwartz@gsfc.nasa.gov.

[4] Naval Research Laboratory, Washington, DC 20375; gerald.share@nrl.navy.mil.

[5] Department of Astronomy, University of Maryland, College Park, MD 20742.

[6] Department of Physics and Santa Cruz Institute for Particle Physics, University of California, Santa Cruz, CA 95064; dsmith@scipp.ucsc.edu.

TABLE 1
RHESSI Neutron-Capture Line Events

Parameter	2003 October 28	2003 October 29	2003 November 2	2002 July 23
GOES class	X17	X10	X8	X4.8
Optical location (deg)	S16, E08	S15, W02	S14, W56	S13, E72
Time range	11:06:20–11:29:40[a]	20:43–21:00	17:16–17:29	00:27:20–00:43:20[b]
2223 ± 5 keV counts in RMCs 6, 9	2280, 1643	463, 313	781, 557	336, 240
2223 ± 5 keV background counts[c]	316, 280	130, 125	121, 118	85, 73
Relative visibility for RMC 6[d]	0.91 ± 0.2[e]	…	0.76 ± 0.26	1.61 ± 0.45
Relative visibility for RMC 9[d]	0.82 ± 0.10	1.28 ± 0.28	0.84 ± 0.15	1.28 ± 0.26
Expected relative visibility for RMC 9[f]	0.90	1.0	0.98	1.0
2.223 MeV source FWHM (arcsec)[g]	<30[h]	<94	<44	<22

[a] Decay phase only.
[b] Expanded since Hurford et al. (2002).
[c] Inferred from nearby continuum.
[d] Ratio of imaged to spatially integrated counts.
[e] Includes both sources.
[f] Based on the RMC 6 image.
[g] 2 σ upper limits, assuming a Gaussian profile.
[h] Each component.

eliminates potential systematic errors that might compromise comparisons. Integration times for the 2.223 MeV images were delayed by 100 s so that the electron-bremsstrahlung and gamma-ray line images would correspond to the same primary particle *interaction* times, although in practice this refinement made no noticeable difference. Where statistics warranted, the CLEAN algorithm (Högbom 1974) was also used on corresponding images to improve sidelobe suppression with no effect on feature location.

2.1. *2003 October 28 Event*

INTEGRAL/SPI observations (Kiener et al. 2006; see our Fig. 1) show that the time profiles of the prompt C and O deexcitation lines (4.4 and 6.1 MeV) and hard X-rays (>150 keV) are closely similar, while the 2.223 MeV profile is delayed by the characteristic ~100 s neutron thermalization time. The *RHESSI* observations begin about 4 minutes after event onset, and they display a smooth exponential decay lasting at least five ~280 s *e*-folding times for the 2.223 MeV line, while the 0.2–0.3 MeV band, dominated by electron bremsstrahlung, has a time profile similar to the >150 keV *INTEGRAL*/SPI hard X-ray profile.

RHESSI's 35″ resolution maps at 0.2–0.3 MeV and at 2.223 MeV (Fig. 2) are both dominated by two compact sources of comparable intensity (fluence ratio of 1.0 ± 0.4) separated by ~80″ and straddling the arcade of loops in the *TRACE* image. The electron-bremsstrahlung sources, however, are displaced by 14″ and 17″ ± 5″ from the 2.223 MeV sources.

With integration times of 1540 s, the images time-average over any footpoint motions. Because of the exponential decay, however, emission in the first few minutes of the interval dominates. For the 0.2–0.3 MeV band, representative locations of the peaks of footpoint locations obtained with shorter time resolutions are indicated by the red plus signs in Figure 2. The general trend was for the east and west footpoints to increase

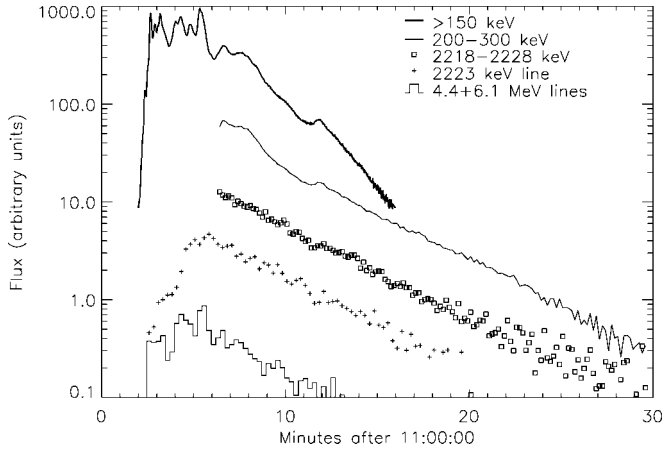

Fig. 1.—Gamma-ray light curves for the 2003 October 28 event from *RHESSI* and *INTEGRAL*/SPI. The *INTEGRAL* data, adapted from Kiener et al. (2006), are shown in the top curve and two lowest curves. The top curve is the dead-time–corrected shield count rate that responds to >150 keV photons. The other curves have been corrected for pre- or postflare levels of background. Line fluences have been corrected for continuum emission. For clarity, the ordinate for each curve has been shifted by an arbitrary factor.

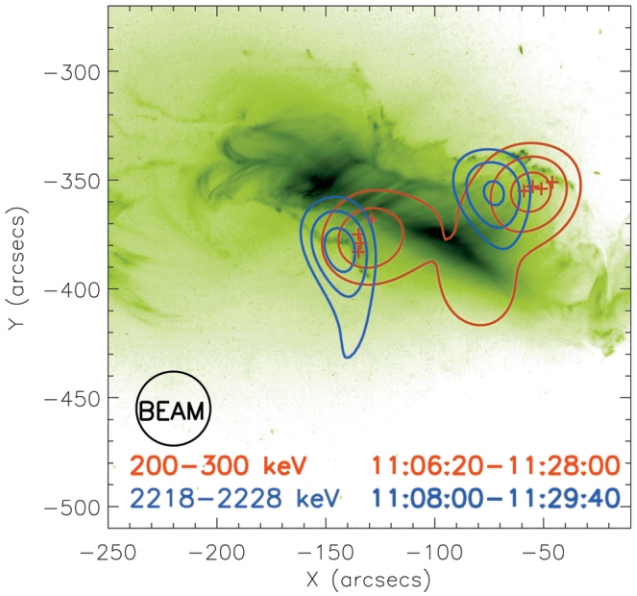

Fig. 2.—Overlay of the 50%, 70%, and 90% contours of 35″ resolution gamma-ray images made with RMCs 6+9 on a *TRACE* 195 Å image of the October 28 flare. The red plus signs indicate 200–300 keV footpoint locations for successive adjacent intervals of 100, 120, 180, and 240 s beginning at 11:06:20. The *X* and *Y* heliographic offsets are positive west and north of Sun center.

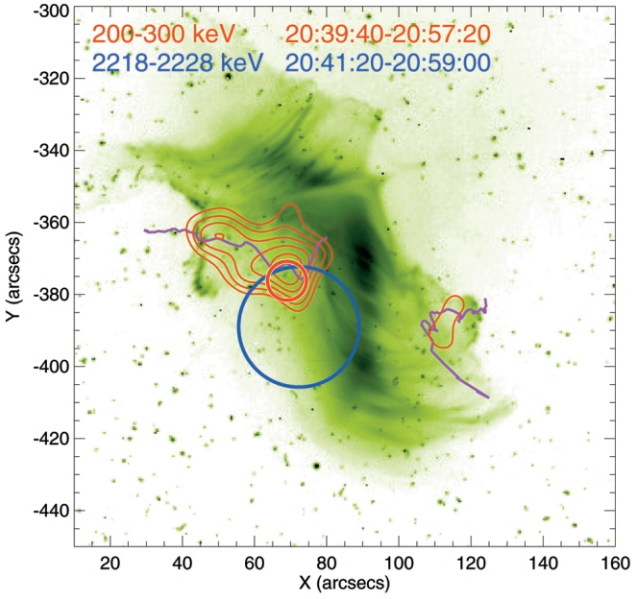

FIG. 3.—The fine red (50%–90%) contours show the 200–300 keV high-resolution map for the 2002 October 29 event superposed on a *TRACE* 195 Å image. The thick red and blue circles are the centroid locations with 1 σ error radii for RMC 9 imaging at 200–300 and 2218–2228 keV, respectively. The purple lines illustrate the motions of the 200–300 keV footpoints.

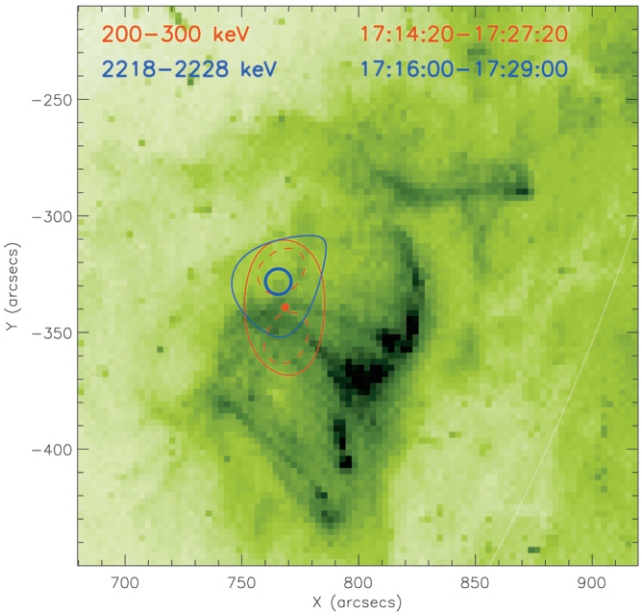

FIG. 4.—Overlay of 200–300 keV (*red contours*) and 2218–2228 keV (*blue contour*) sources onto a postflare *SOHO*/EIT image for the 2002 November 2 event. The dashed and thin solid red 50% contours show the result of 200–300 keV mapping with 7″ and 35″ resolution (RMCs 3–9 and 6+9), respectively. The 35″ map cannot quite resolve the double-footpoint source revealed by the high-resolution map and so has an elongated profile. The thin blue 50% contour is the corresponding RMC 6+9 map at 2218–2228 keV. The thicker 1 σ error circles show the RMC 6 source centroid locations.

their separation, moving ~15″ toward the south and west, respectively. Only an upper limit of ~30″ could be placed on potential motions of the centroids of the 2.223 MeV footpoints.

2.2. *2003 October 29 Event*

The 2003 October 29 event, observed in its entirety by *RHESSI*, had a high and variable background from penetrating energetic particles precipitating from the radiation belts. Since background is not modulated by the grids, this did not impair imaging of the flare. The hard X-ray observations (Krucker et al. 2005) initially showed multiple sources that became two sources with generally outward motions straddling the loop arcade seen by *TRACE*. Figure 3 shows the 0.2–0.3 MeV hard X-ray image, integrated over the flare, with the motion of the footpoints indicated by the purple lines. Although the 2.223 MeV imaging with RMC 6 did not yield a statistically significant result for this flare, RMC 9 imaging with 183″ resolution showed an unresolved source whose centroid location is shown as the dark blue circle with a 17″ 1 σ error radius. The apparent 13″ displacement from the corresponding 0.2–0.3 MeV emission centroid (*solid red circle*) is not statistically significant.

2.3. *2003 November 2 Event*

The 2003 November 2 event was well observed, and the 50% contours of the resulting gamma-ray images are shown in Figure 4 superposed on a postflare *SOHO*/EIT image.

Imaging the 0.2–0.3 MeV hard X-ray emission with RMCs 3 through 9 (7″ resolution) showed two equal footpoints separated by 29″ (*dashed red 50% contours*) straddling a Michelson Doppler Imager (MDI) magnetic neutral line running south-southwest to north-northwest. Images with only RMC 6 (35″ FWHM) did not have sufficient resolution to separate the footpoints, and so they appear as a single elongated source (*solid red contour*) centered between the footpoints.

The corresponding RMC 6 2.223 MeV line image is shown as the thin blue 50% contour. Its centroid, shown as the thick blue circle with a 1 σ error radius, is displaced by 11″ ± 5″ from the corresponding centroid of the 0.2–0.3 MeV RMC 6 image (*small red circle*). Its location suggests that the 2.223 MeV line source may be preferentially associated with the more northerly footpoint.

3. DISCUSSION

In common with flare-accelerated electrons, ions accelerated by a flare would be expected to interact at footpoint locations, whereas ions accelerated by a CME shock would be expected to be widely dispersed and/or displaced from the flare site. The latter possibility was suggested by the detection of the 2.223 MeV line in an over-the-limb flare event (Vestrand & Forrest 1993). Since the three flares studied here all had associated fast CMEs with SEP events observed at 1 AU (Mewaldt et al. 2005), they are potential candidates for such behavior. The present observations provide us with an opportunity to distinguish between the two possibilities. Specifically, the photon flux of a source that is significantly smaller than the RMC angular resolution would be completely modulated, resulting in a relative visibility (defined as the ratio of the modulated flux to spatially integrated flux) close to unity, whereas an extended source much larger than the RMC angular resolution would be only weakly modulated, with a relative visibility close to zero. Spatially integrated counts are determined by summing the counts between 2.218 and 2.228 MeV and subtracting the background contribution inferred from simultaneously observed continuum counts in the same detector at energies between 2.24 and 2.30 MeV. Note that potential uncertainties in either the detector efficiency or a specific background model do not affect the relative visibility measurement. For all three events, the RMC 9 relative visibility at 2.223 MeV is consistent with 1, implying

compact sources (Table 1). Assuming Gaussian profiles, the relative visibilities implied sizes of a few tens of arcseconds or less. Furthermore, in all four *RHESSI*-imaged events (including 2002 July 23), the 2.223 MeV sources are located within the flaring active region. We conclude that for all the imaged events, the gamma-ray–producing ions are locally accelerated by the flare and not by the associated fast CME shock.

Further evidence for flare-accelerated ions is the first observation (October 28) of a double source, one that straddles the flaring loop arcade, a characteristic typical of electron-bremsstahlung footpoint sources. In contrast, the other three flares imaged to date have yielded only single unresolved sources. However, to image a double source with a 35″ resolution RMC, the footpoints must be separated by at least 35″, and the signal-to-noise ratio (S/N) must be sufficient to support detection of each component. For a given subcollimator, the statistical S/N scales as the ratio of the number of each component's source counts to the square root of the total number of counts. Based on this measure, the October 28 event had 2–3 times the S/N of each of the other events. Furthermore, in two of the other cases (October 29 and November 2), the footpoint separation, as indicated by electron-bremsstrahlung images, was too small to be resolved by RMC 6. Therefore, a double source could not have been detected in any of the other events.

Turning to the issue of the relative locations of the ion- and electron-associated sources, one result of previous gamma-ray imaging (Hurford et al. 2003) was the displacement of the centroid of the 2.223 MeV source in the 2002 July 23 event from that of the electron-bremsstrahlung source. For the October 28 flare, the two separate 2.223 MeV footpoints on opposite sides of the flaring loop arcade were displaced from the corresponding 0.2–0.3 MeV electron-bremsstrahlung footpoints by 14″ and 17″ ± 5″. For the October 29 event, the displacement (if any) between the centroid of the 2.223 MeV source and that of the 0.2–0.3 MeV sources is 13″ ± 18″. For the November 2 event, there is an 11″ ± 5″ displacement of the centroid of the 2.223 MeV source toward the northerly 0.2–0.3 MeV electron-bremsstrahlung component, with the 2.223 MeV source seeming to favor one of the two electron-bremsstrahlung footpoints. Following the initial analysis of the 2002 July 23 event (Hurford et al. 2003), an improved roll aspect solution became available that enabled the entire flare to be imaged rather than the more limited interval reported previously. The revised analysis (Table 1) confirmed the original result, with the 20″ ± 6″ displacement previously reported becoming a 25″ ± 5″ displacement when the longer integration time was used.

These displacements imply spatial differences in the acceleration and/or transport of energetic electrons and ions in solar flares. To account for this, Emslie et al. (2004a) discussed a stochastic acceleration mechanism whereby the ions are preferentially accelerated in larger loops than the electrons. This was consistent with the observation (Lin et al. 2003) that the ion source location in the 2002 July 23 event was near the footpoints of a larger arcade of postflare loops while the electron sources were at the footpoints of a smaller arcade of loops. In the October 28 event, however, the two 2.223 MeV gamma-ray line footpoint sources have about the same separation as the two 0.2–0.3 MeV electron-bremsstrahlung footpoint sources.

Alternatively, if all the particles are accelerated in a single source, gradient and curvature drifts of the electrons and ions in opposite directions along the flare magnetic arcade can produce displacement. In the October 28 event, the *SOHO*/MDI magnetograph indicates the arcade magnetic fields run south to north, implying that energetic ions will drift eastward and electrons westward, consistent with the direction of the observed displacement of the footpoints. The drift speed is given approximately by $v_d \sim E/qBR_c$ (Chen 1984, p. 26), where E, q, B, and R_c are the particle kinetic energy, particle charge, magnetic field strength, and radius of curvature of the field, respectively. For an estimated arcade field of $B \sim 100$ G and $R_c \sim 40''$, v_d is ~100 m s^{-1} for 30 MeV protons and ~1 m s^{-1} for 0.3 MeV electrons. For the flare duration of 10^3 s, these drifts would therefore produce a displacement of only ~10^2 km, about 2 orders of magnitude smaller than the observed displacement.

Another alternative is suggested by theoretical studies whereby the acceleration of particles by strong electric fields in a current sheet formed by reconnecting loops (Litvinenko & Somov 1993, 1995) can lead to separation of particles with opposite charge (Zharkova & Gordovskyy 2004). However, it is not clear whether this is consistent with the displacements reported here.

In summary, it would seem that at this stage, the observed displacements are not understood. Our current, rather sketchy picture of the spatial characteristics of flare-accelerated nuclei clearly would benefit from gamma-ray observations with better spatial resolution and sensitivity, and of course by the observation of additional gamma-ray flares.

We thank the *TRACE* and *SOHO*/EIT teams for making their images conveniently accessible and J. Kiener for kindly supplying *INTEGRAL*/SPI results in digital form. This work has been supported by NASA contracts NAS5-98033 and NNG05G189G.

REFERENCES

Chen, F. F. 1983, Introduction to Plasma Physics and Controlled Fusion, Vol. 1: Plasma Physics (2nd ed.; New York: Plenum)
Emslie, A. G., Dennis, B. R., Holman, G. D., & Hudson, H. S. 2005, J. Geophys. Res., 110, A11103
Emslie, A. G., Miller, J. A., & Brown, J. C. 2004a, ApJ, 602, L69
Emslie, A. G., et al. 2004b, J. Geophys. Res., 109, A10104
Högbom, J. A. 1974, A&AS, 15, 417
Hua, X.-M., & Lingenfelter, R. E. 1987, Sol. Phys., 107, 351
Hurford, G. J., Schwartz, R. A., Krucker, S., Lin, R. P., Smith, D. M., & Vilmer, N. 2003, ApJ, 595, L77
Hurford, G. J., et al. 2002, Sol. Phys., 210, 61
Kahler, S. 1994, ApJ, 428, 837
Kiener, J., Gros, M., Tatischeff, V., & Weidenspointer, G. 2006, A&A, 445, 725
Krucker, S., Fivian, M. D., & Lin, R. P. 2005, Adv. Space Res., 35, 1707
Lin, R. P., & Hudson, H. S. 1976, Sol. Phys., 50, 153
Lin, R. P., et al. 2002, Sol. Phys., 210, 3
———. 2003, ApJ, 595, L69
Litvinenko, Y. E., & Somov, B. V. 1993, Sol. Phys., 146, 127
———. 1995, Sol. Phys., 158, 317
Mewaldt, R. A., et al, 2005, J. Geophys. Res., 110, A09S18
Ramaty, R., Kozlovsky, B., & Lingenfelter, R. E. 1979, ApJS, 40, 487
Ramaty, R., & Mandzhavidze, N. 2000, in IAU Symp. 195, Highly Energetic Physical Processes and Mechanisms for Emission from Astrophysical Plasmas, ed. P. C. H. Martens, S. Tsuruta, & M. A. Weber (San Francisco: ASP), 123
Ramaty, R., Mandzhavidze, N., Kozlovsky, B., & Murphy, R. 1995, ApJ, 455, L193
Share, G. H., & Murphy, R. J. 2004, in IAU Symp. 219, Stars as Suns: Activity, Evolution and Planets, ed. A. K. Dupree & A. O. Benz (San Francisco: ASP), 133
Smith, D. M., Share, G. H., & Murphy, R. J., Schwartz, R. A., Shih, A. Y., & Lin, R. P. 2003, ApJ, 595, L81
Smith, D. M., et al. 2002, Sol. Phys., 210, 33
Vestrand, W. T., & Forrest, D. J. 1993, ApJ, 409, L69
Zharkova, V. V., & Gordovskyy, M. 2004, ApJ, 604, 884